Electronic Supplementary Material (ESI) for Journal of Materials Chemistry C.

Coexistence of long-range ferromagnetic ordering and spin-glass behavior observed in the first inorganic–organic hybrid 1-D oxalate-bridging nona-Mn^{II} sandwiched tungstoantimonate chain

Jiancai Liu,[a] Jie Luo,[a] Qing Han,[a] Jing Cao,[a] Lijuan Chen,[a,]* You Song[a,b,]* and Junwei Zhao[a,c,]*

[a]Henan Key Laboratory of Polyoxometalate Chemistry, Institute of Molecular and Crystal Engineering, College of Chemistry and Chemical Engineering, Henan University, Kaifeng, Henan 475004, P. R. China

[b]State Key Laboratory of Coordinate Chemistry, Collaborative Innovation Center of Advanced Microstructures, School of Chemistry and Chemical Engineering, Nanjing University, Nanjing 210093, China. Email: yousong@nju.edu.cn

[c]State Key Laboratory of Structural Chemistry, Fujian Institute of Research on the Structure of Matter, Chinese Academy of Sciences, Fuzhou, Fujian 350002, P. R. China

Fig. S12 The hysteresis loop for **1** measured at 2 K at a sweeping rate of 100 Oe s^{-1}.

Fig. S13 (a) The TG and DTG curves of **1**. Insert: the DTA curve of **1**. (b) The variable-temperature IR spectra of **1**.

Fig. S14 (a) The UV spectrum of **1**. (b) The UV spectrum of the $Na_9[B\text{-}\alpha\text{-}SbW_9O_{33}]\cdot 19.5H_2O$ precursor.

Table S1. Bond valence sum (BVS) calculations for W, Sb and Mn centers.

Table S2. Selected bond lengths [Å] and angles [°] for **1**.

The structural refinement details of 1

Because of the large structure of **1** and the existence of a large amount of weight atoms, the intensity data are not very good, leading to the ADP max/min ratio of some atoms, and it is very difficult to refine this large structure, therefore, some unit-occupancy atoms have been refined isotropically and restrainedly refined. O6W-O8W and N6 are refined isostropicallly. 636 parameters and 1 restraint is used in the refinement.

Recent progress on main-group metal or lanthanide substituted TAs

The research on the realm of TAs has aroused considerable attention for a long time. A very interesting family of main group (MG) metal inserted POMs that are derived from the substitution of MG metal atoms (most of them are Na^+ or K^+ ions) in place of other metal ions in the central belt has been extensively studied.[1] Recently, the reports on MG-containing TAs have been expanded to the Ga-/Sn-based species besides these common Na^+ or K^+ ions involving $[Ga_4(H_2O)_{10}(\beta\text{-}SbW_9O_{33})_2]^{6-}$ and $[\{Na(\mu\text{-}OH_2)(OH_2)_2\}_6\{Sn_6(B\text{-}SbW_9O_{33})_2\}_2]^{6-}$.[2] Compared with the tremendous number of TMSPs, the discoveries on lanthanide (Ln)-substituted TAs are relatively scarce, and the majority of them are inorganic and isolated structures, such as the Krebs-type TAs supported by mono-, di- and tetra-Ln ions referring to $[Ln(H_2O)_4Sb_2W_{21}O_{72}(OH)]^{10-}$ (Ln = Yb^{III}, Lu^{III}), $[Ln_2(H_2O)_8Sb_2W_{20}O_{70})]^{8-}$ (Ln = Yb^{III}, Lu^{III}, Y^{III}) and $[\{Y(H_2O)_7\}_4Sb_2W_{22}O_{76}]^{2-}$,[3a,b] the mixed-polyoxotungstate anion $[Eu_3(H_2O)_3(SbW_9O_{33})(W_5O_{18})]^{l8-}$,[3c] and the tetrameric aggregate $[(SbW_9O_{33})_4\{WO_2(H_2O)\}_2Ce_3(H_2O)_8(Sb_4O_4)]^{19-}$.[3d] In 2011, a novel acetate-decorated Y^{III}-containing trimer with a tetrahedral WO_4^{2-} capping unit $[\{Y(\alpha\text{-}SbW_9O_{31}(OH)_2)(CH_3COO)(H_2O)\}_3(WO_4)]^{17-}$ was addressed by Kortz's lab.[3e] Afterwards, two types of inorganic-organic hybrid Ln-substituted TAs $[Ln_2(H_2O)_4\{WO_2(pic)\}_2(SbW_8O_{30})_2]^{10-}$ (Ln = La^{III}, Pr^{III}) and $[\{Ln(H_2O)\}\{Ln(pic)\}(Sb_3O_4)(SbW_8O_{31})(SbW_{10}O_{35})]_2^{24-}$ (Ln = Tb^{III}, Dy^{III}, Ho^{III}) have been triumphantly obtained by Wang's group.[3f] Our group has launched immense exploration on the TM/Ln/POM system and several types of TM–Ln-substituted POMs have been isolated. In 2014, our group succeeded in prepapring the first inorganic–organic TA hybrids comprising TM, Ln and thr ingredients $[Ln(H_2O)_8]_2[Fe_4(H_2O)_8(thr)_2][B\text{-}\beta\text{-}SbW_9O_{33}]_2\cdot 22H_2O$ (Ln = Pr^{III}, Nd^{III}, Sm^{III}, Eu^{III}, Gd^{III}, Dy^{III}, Lu^{III}, thr = threonine). [4a] Later, a series of inorganic TM–Ln-substituted TAs were successively reported by our group.[4b] From then on, great interest on the design and assembly of TM–Ln-substituted TAs has been stimulated. In 2015, Zhang et al obtained a ring-like 3d–4f–4p cluster-containing TA $\{K_2Dy_2Cu_2(H_2O)_8(SbW_9O_{33})_2\}^{6-}$.[4c] In 2016, Reinoso et al isolated a series of of tetrameric TA aggregates $[Sb_7W_{36}O_{133}Ln_3M_2(OAc)(H_2O)_8]^{17-}$ (Ln = La^{III} – Gd^{III}, M = Co^{II}; Ln = Ce^{III}, M = Ni^{II} and Zn^{II}).[4d] Thus, in the future, much more work is to be done in constructing TA-based metal-oxo clusters.

1 J. C. Liu, Q. Han, L. J. Chen and J. W. Zhao, *CrystEngComm*, 2016, **18**, 842.

2 (a) B. Kandasamy, S. Vanhaecht, F. M. Nkala, T. Beelen, B. S. Bassil, T. N. Parac-Vogt and U. Kortz, *Inorg. Chem.*, 2016, **55**, 9204; (b) C. C. Zhao, E. N. Glass, B. Chica, D. G. Musaev, J. M. Sumliner, R. B. Dyer, T. Q. Lian and C. L. Hill, *J. Am. Chem. Soc.*, 2014, **136**, 12085.

3 (a) A. H. Ismail, B. S. Bassil, I. Römer and U. Kortz, *Z. Anorg. Allg. Chem*., 2013, **639**, 2510; (b) R. X. Tan, X. H. Pang, Y. L. Ren, X. H. Wang and R. Li, *Z. Anorg. Allg. Chem*., 2011, **637**, 1178; (c) T. Yamase, H. Naruke and Y. Sasaki, J. Chem. Soc. *Dalton Trans*., 1990, 1687; (d) G. L. Xue, J. Vaissermann and P. Gouzerh, *J. Cluster Sci.,* 2002, **13**, 409; (e) M. Ibrahim, S. S. Mal, B. S. Bassil, A. Banerjee, and U. Kortz, *Inorg. Chem*., 2011, **50**, 956; (f) L.-L. Li, H.-Y. Han, Y.-H.Wang, H.-Q. Tan, H.-Y. Zang and Y.-G. Li, *Dalton Trans*., 2015, **44**, 11429.

4 (a) J.-W. Zhao, J. Cao, Y.-Z. Li, J. Zhang and L.-J. Chen, *Cryst. Growth Des*., 2014, **14**, 6217; (b) L. J. Chen, J. Cao, X. H. Li, X. Ma, J. Luo and J. W. Zhao, *CrystEngComm*, 2015, **17**, 5002; (c) S. Yao, J.-H. Yan, H. Duan, Q.-Q. Jia, Z.-M. Zhang and E.-B. Wang, *RSC Adv*., 2015, 5, 76206; (d) B. Artetxe, S. Reinoso, L. S. Felices, L. Lezama, J. M. Gutiérez-Zorrilla, C. Vicent, F. Haso and T. B. Liu, *Chem. Eur. J*., 2016, **22**, 4616.

TG, DTG, DTA analyses and variable-temperature IR spectra

In order to examine the thermal properties, the TG, DTG and DTA analyses of **1** were performed on polycrystalline samples under the N_2 atmosphere in the temperature range of 25–800 °C at a heating rate of 10 °C min^{-1} (Fig. S13a). On the whole, the TG curve of **1** shows a two-step weight loss. An initial rapid weight loss of 11.07 % from ambient temperature to 310 °C can be attributed to the removal of thirty none lattice water molecules and nine coordinated water molecules (calcd 11.56 %). Further heating until 800 °C leads to the decomposition of the framework with a second weight loss of 5.60 %, roughly corresponding to the release of the remaining five coordinated water molecules, the dehydration of four protons and the departure of six carbon dioxides derived from the destruction of oxalate ligands (calcd 6.26 %). Two evident peaks are observed from the DTG curve in the range of 25–250 °C and 330–470 °C, implying two rapid weight-loss stages in the thermal decomposition of **1**, which well conforms to the TG curve. Correspondingly, one endothermal peak observed at 84.7 °C in the DTA curve results from the release of lattice water molecules in the first weight loss while the strong exothermal peak at 401.7 °C probably arises from the loss of organic molecules. The broad exothermal peak at 705.3 °C suggests the decomposition of the polyoxoanion skeleton.[1]

Additionally, the variable-temperature IR spectra have been performed on the basis of the TG results in order to gain a better understanding of the thermal decomposition procedure of **1** (Fig. S13b). Obviously, the characteristic vibration bands of **1** remain unchanged when temperature rises from 25 to 380 °C, indicating that the polyoxoanionic skeleton of **1** is stable in this temperature range in spite of the release of some water molecules, which is in good accordance with the first weight loss of the TG analysis. A further heating to 450 °C leads to the gradual disappearance of the $\nu_{as}(CO_2^-)$ and $\nu_s(CO_2^-)$ vibration bands as well as the weakening of the $\nu(Sb-O_a)$, $\nu(W-O_t)$, $\nu(W-O_b)$ and $\nu(W-O_c)$ vibration bands, revealing the destruction of oxalate ligands. This result matches well with the exothermal peak at 401.7 °C in the DTA curve. After 600 °C, the $\nu_{as}(CO_2^-)$ and $\nu_s(CO_2^-)$ peaks have vanished and the characteristic peaks derived from the $[B\text{-}\alpha\text{-}SbW_9O_{33}]^{9-}$ fragments become invisible, which demonstrates that the main skeleton of **1** is not maintained, in supporting with the TG profile of the dehydration of protons leading to the destruction of the polyoxoanionic framework.

1 S. F. West and L. F. Audrieth, *J. Phys. Chem.,* 1955, **59**, 1069.

UV spectra

The UV spectrum of **1** was measured in the aqueous solution in the range of 190–400 nm, which exhibits one strong absorption band centered at 192 nm and a looming band at around 270 nm (Fig. S14a). The higher energy absorption band can be attributed to the pπ–dπ charge-transfer transitions of the $O_t \rightarrow W$ bonds derived from the $[B\text{-}\alpha\text{-}SbW_9O_{34}]^{9-}$ skeletons whereas the lower energy absorption band can be assigned to the pπ–dπ charge-transfer transitions of the $O_{b,c} \rightarrow W$ bonds of the $[B\text{-}\alpha\text{-}SbW_9O_{34}]^{9-}$ skeletons.[1] This assignment was further consolidated by the UV spectrum of the $Na_9[B\text{-}\alpha\text{-}SbW_9O_{33}]\cdot 19.5H_2O$ precursor with two absorption bands located at 194 nm and 275 nm, respectively (Fig.

S14b). In comparison with the $Na_9[B\text{-}\alpha\text{-}SbW_9O_{33}]\cdot19.5H_2O$ precursor, two absorption bands of the UV spectrum of **1** are slightly blue-shifted, which probably results from the implantation of the $\{[Mn(H_2O)_3]_3[Mn(H_2O)_2]_2[Mn(H_2O)][Mn(C_2O_4)]_3\}^{12+}$ cluster into the sandwich belt of **1**.

1 (a) J. Y. Niu, K. H. Wang, H. N. Chen, J. W. Zhao, P. T. Ma, J. P. Wang, M. X. Li, Y. Bai and D. B. Dang, *Cryst. Growth Des*., 2009, **9**, 4362; (b) N. V. Izarova, L. Klaß, P. de Oliveira, I.-M. Mbomekalle, V. Peters, F. Haarmann and P. Kögerler, *Dalton Trans*., 2015, **44**, 19200.

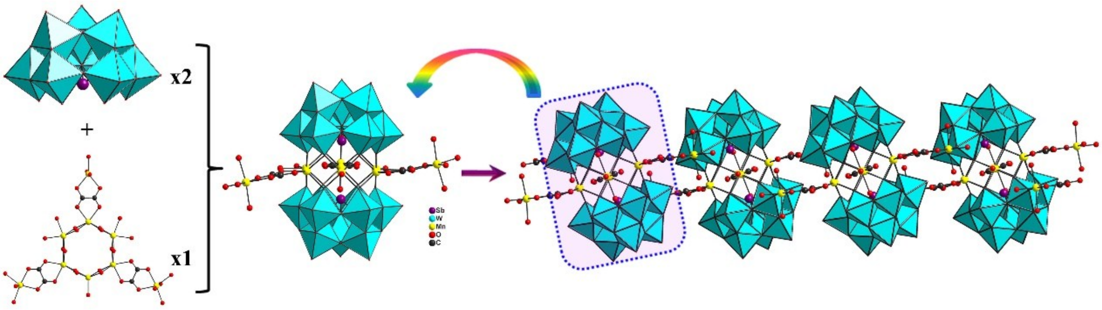

Fig. S1 The schematic combination process of **1**.

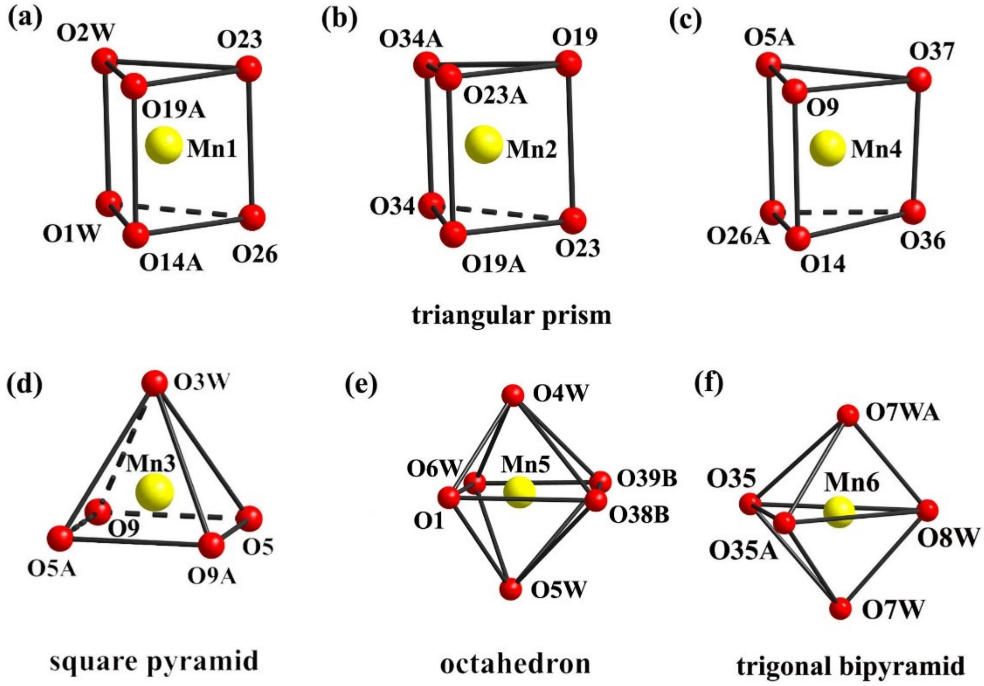

Fig. S2 (a)–(c) The hexa-coordinate triangular prism geometries of $Mn1^{2+}$, $Mn2^{2+}$ and $Mn4^{2+}$ ions. (d) The penta-coordinate square pyramid configuration of $Mn3^{2+}$ ion. (e) The hexa-coordinate octahedral motif of $Mn5^{2+}$ ion. (f) The penta-coordinate trigonal bipyramid configuration of $Mn6^{2+}$ ion. Symmetry codes: A: $1-x, y, 0.5-z$; B: $x, -1-y, 0.5+z$.

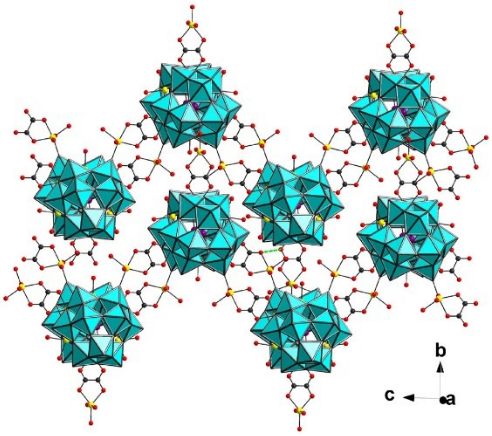

Fig. S3 The weak π···π stacking between contiguous oxalate ligands with the distance of 6.57 Å. The light green bonds highlight the π···π interactions.

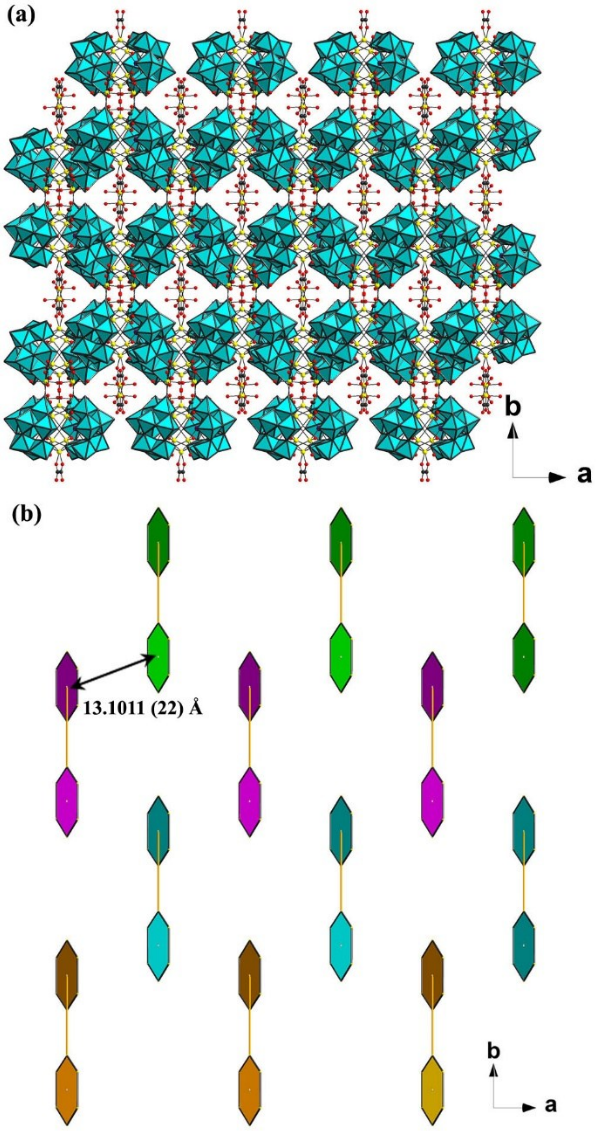

Fig. S4 (a)The 3-D packing architecture; (b) The simplified 3-D packing mode of **1** viewed along *c* axis with the interchain distance of 13.10 Å.

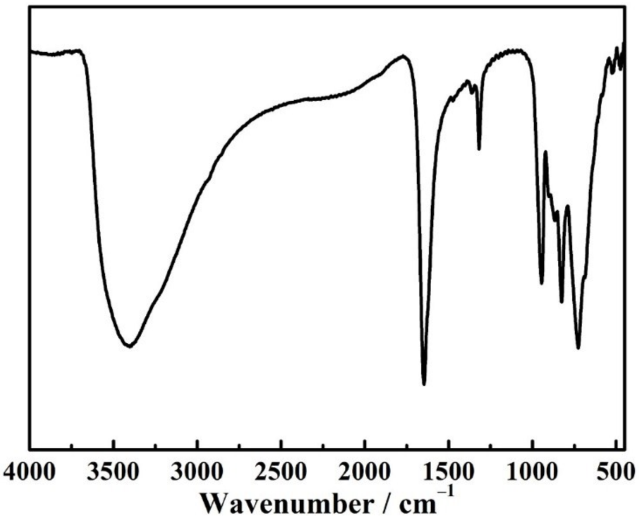

Fig. S5 The IR spectrum of **1**.

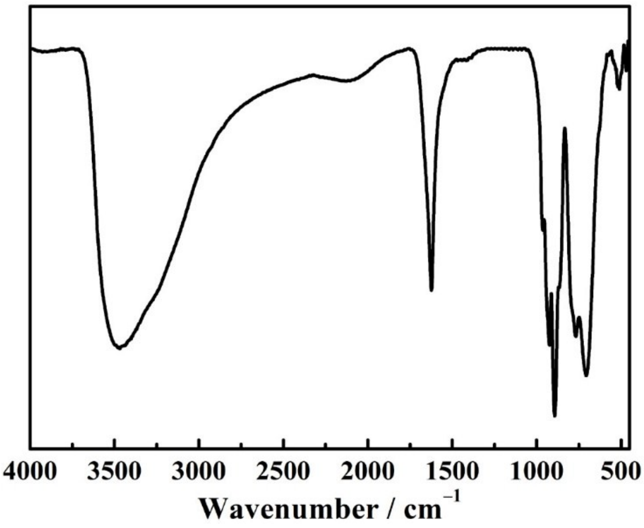

Fig. S6 The IR spectrum of the [B-α-SbW_9O_{33}]$^{9-}$ precursor.

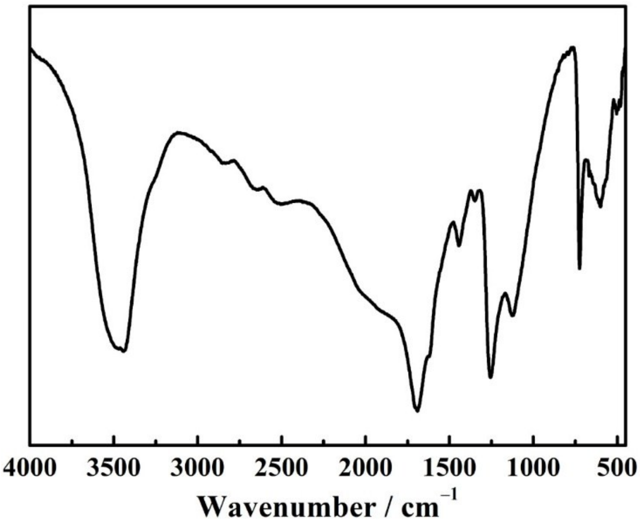

Fig. S7 The IR spectrum of free oxalic acid ligand.

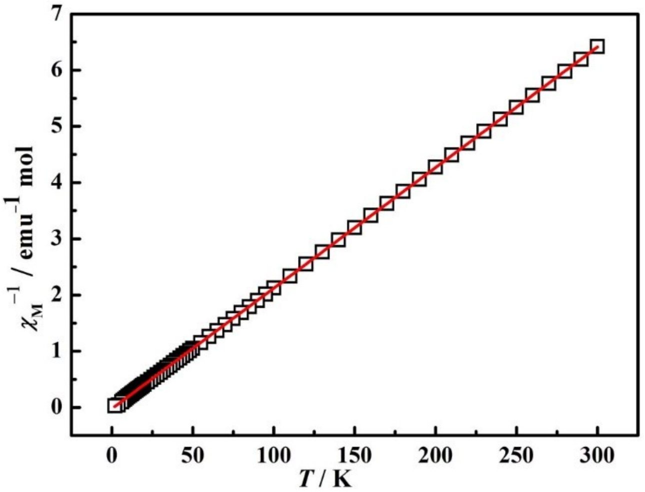

Fig. S8 The plot of χ_M^{-1} *vs*. T between 2 and 300 K for **1**. The red solid line is fitted by the Curies–Weiss law.

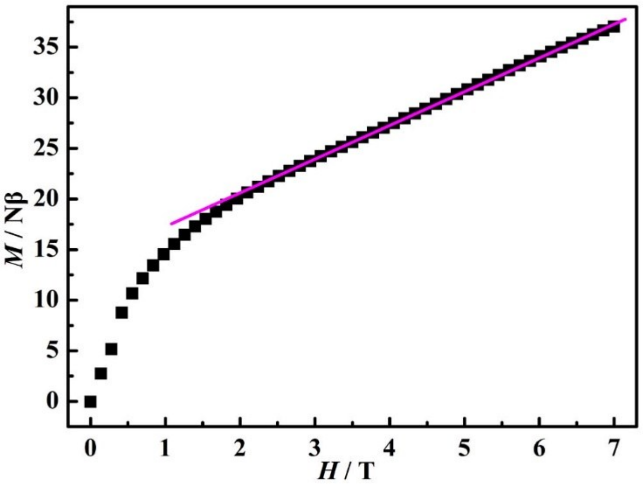

Fig. S9 Field dependence of magnetization of **1** at 2K.

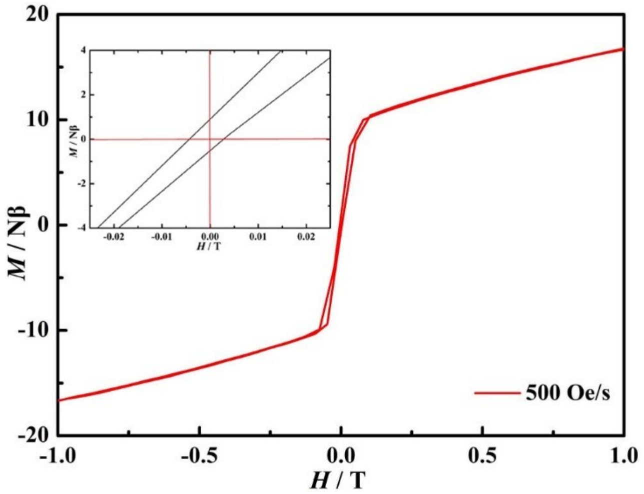

Fig. S10 The hysteresis loop for **1** measured at 2 K at a sweeping rate of 500 Oe s^{-1}. Insert: the magnification of the hysteresis loop for **1**.

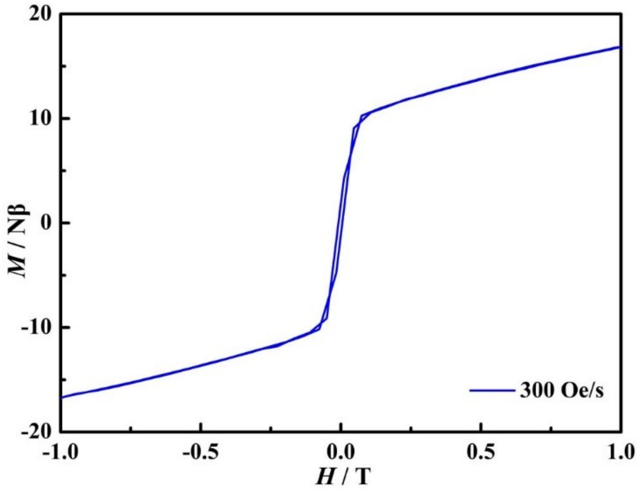

Fig. S11 The hysteresis loop for **1** measured at 2 K at a sweeping rate of 300 Oe s^{-1}.

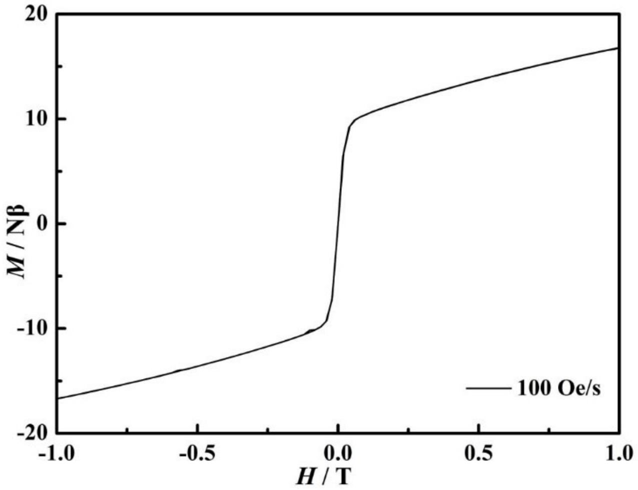

Fig. S12 The hysteresis loop for **1** measured at 2 K at a sweeping rate of 100 Oe s^{-1}.

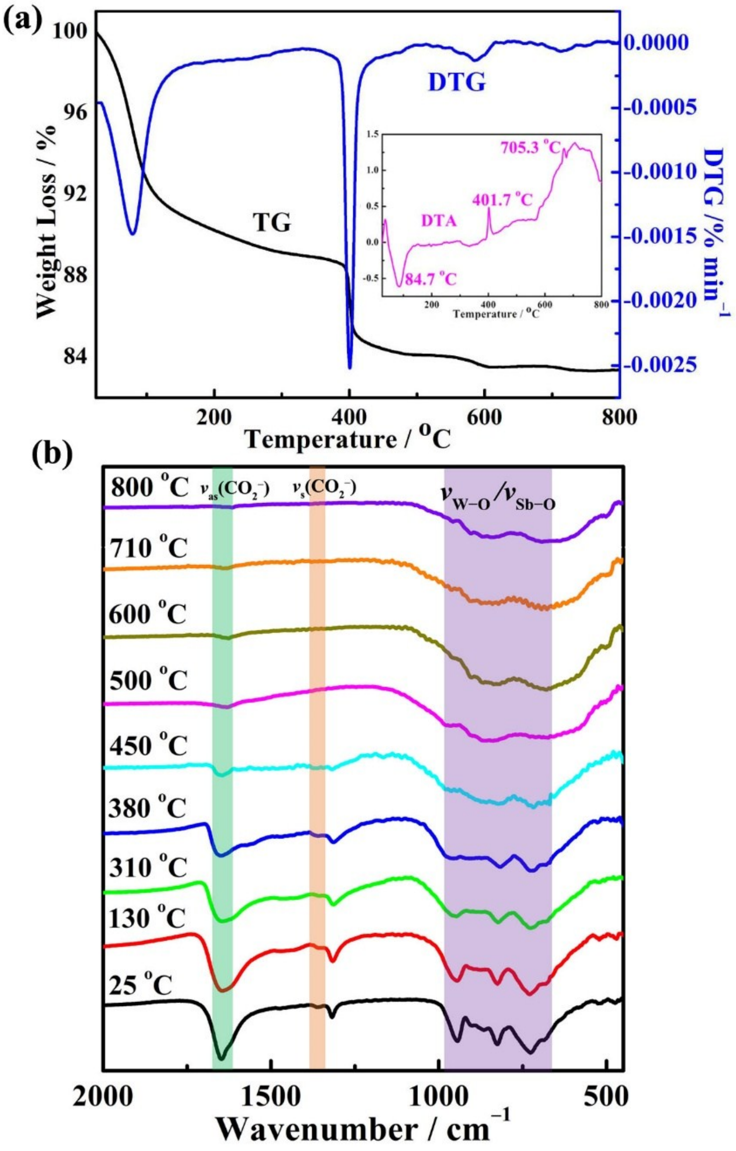

Fig. S13 (a) The TG and DTG curves of **1**. Insert: the DTA curve of **1**. (b) The variable-temperature IR spectra of **1**.

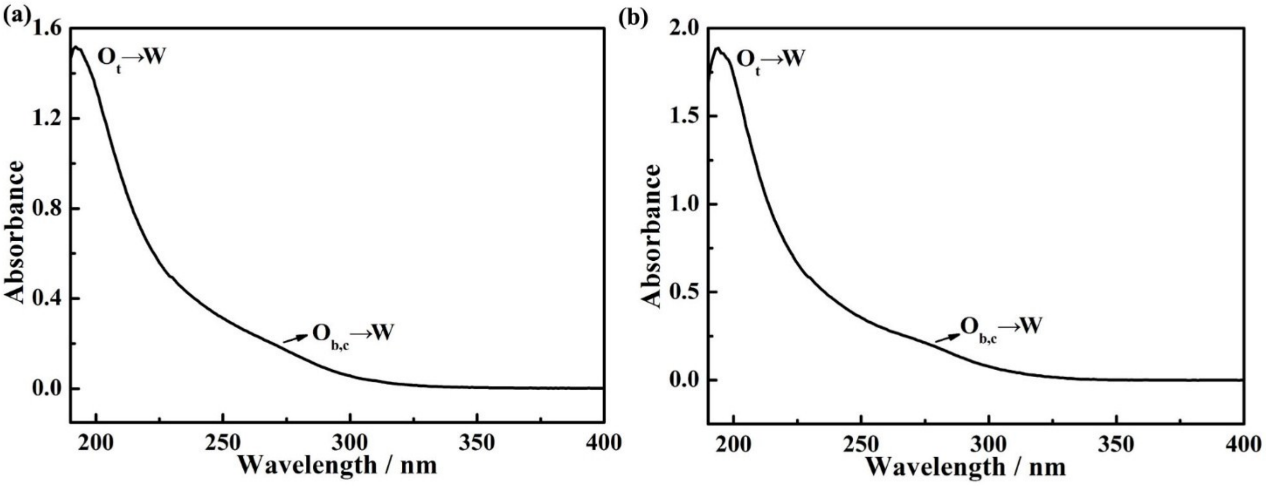

Fig. S14 (a) The UV spectrum of **1**. (b) The UV spectrum of the $Na_9[B\text{-}\alpha\text{-}SbW_9O_{33}]\cdot 19.5H_2O$ precursor.

Table S1 Bond valence sum (BVS) calculations for W, Sb and Mn centers.

Atom	BVS	Atom	BVS
W1	5.96	Mn1	2.07
W2	6.25	Mn2	2.00
W3	6.02	Mn3	2.02
W4	6.04	Mn4	1.89
W5	6.01	Mn5	2.10
W6	6.05	Sb1	2.88
W7	6.11		
W8	6.11		
W9	6.09		

Table S2 Selected bond lengths [Å] and angles [°] for **1**.

Mn(1)–O(23)	2.144(11)	O(23)–Mn(1)–O(14)#1	131.6(4)	O(36)–Mn(4)–O(26)#1	81.5(4)
Mn(1)–O(19)#1	2.176(10)	O(19)#1–Mn(1)–O(14)#1	81.3(4)	O(9)–Mn(4)–O(26)#1	132.9(4)
Mn(1)–O(26)	2.181(9)	O(26)–Mn(1)–O(14)#1	79.1(3)	O(5)#1–Mn(4)–O(26)#1	83.6(4)
Mn(1)–O(14)#1	2.190(9)	O(23)–Mn(1)–O(2W)	85.6(4)	O(36)–Mn(4)–O(14)	85.0(4)
Mn(1)–O(2W)	2.210(10)	O(19)#1–Mn(1)–O(2W)	84.2(4)	O(9)–Mn(4)–O(14)	83.3(3)
Mn(1)–O(1W)	2.211(11)	O(26)–Mn(1)–O(2W)	137.9(4)	O(5)#1–Mn(4)–O(14)	132.6(3)
Mn(2)–O(19)#1	2.182(9)	O(14)#1–Mn(1)–O(2W)	135.5(4)	O(26)#1–Mn(4)–O(14)	77.4(3)
Mn(2)–O(19)	2.182(9)	O(23)–Mn(1)–O(1W)	136.3(4)	O(36)–Mn(4)–O(37)	73.5(4)
Mn(2)–O(23)#1	2.204(10)	O(19)#1–Mn(1)–O(1W)	136.8(4)	O(9)–Mn(4)–O(37)	88.6(4)
Mn(2)–O(23)	2.204(10)	O(26)–Mn(1)–O(1W)	85.1(4)	O(5)#1–Mn(4)–O(37)	87.2(4)
Mn(2)–O(34)#1	2.209(11)	O(14)#1–Mn(1)–O(1W)	86.0(4)	O(26)#1–Mn(4)–O(37)	133.9(4)
Mn(2)–O(34)	2.209(11)	O(2W)–Mn(1)–O(1W)	76.6(4)	O(14)–Mn(4)–O(37)	136.0(4)
Mn(3)–O(3W)	2.08(3)	O(19)#1–Mn(2)–O(19)	133.5(5)	O(4W)–Mn(5)–O(1)	86.9(4)
Mn(3)–O(9)#1	2.127(10)	O(19)#1–Mn(2)–O(23)#1	84.8(4)	O(4W)–Mn(5)–O(5W)	170.8(7)
Mn(3)–O(9)	2.127(10)	O(23)#1–Mn(2)–O(23)	134.0(5)	O(1)–Mn(5)–O(5W)	87.2(6)
Mn(3)–O(5)#1	2.147(9)	O(19)#1–Mn(2)–O(34)#1	135.7(4)	O(4W)–Mn(5)–O(38)#2	94.7(6)
Mn(3)–O(5)	2.147(9)	O(19)–Mn(2)–O(34)#1	85.2(4)	O(1)–Mn(5)–O(38)#2	96.9(4)
Mn(4)–O(36)	2.188(10)	O(23)#1–Mn(2)–O(34)#1	84.5(4)	O(5W)–Mn(5)–O(38)#2	93.2(6)
Mn(4)–O(5)#1	2.210(10)	O(23)–Mn(2)–O(34)#1	136.2(4)	O(4W)–Mn(5)–O(39)#2	90.2(5)
Mn(4)–O(26)#1	2.225(9)	O(19)#1–Mn(2)–O(34)	85.2(4)	O(1)–Mn(5)–O(39)#2	171.2(4)
Mn(4)–O(14)	2.225(9)	O(19)–Mn(2)–O(34)	135.7(4)	O(5W)–Mn(5)–O(39)#2	96.6(6)
Mn(4)–O(37)	2.246(11)	O(23)#1–Mn(2)–O(34)	136.2(4)	O(38)#2–Mn(5)–O(39)#2	74.9(4)
Mn(4)–O(9)	2.209(10)	O(23)–Mn(2)–O(34)	84.5(4)	O(4W)–Mn(5)–O(6W)	87.5(6)

Mn(5)–O(4W)	2.150(14)	O(34)#1–Mn(2)–O(34)	73.7(7)	O(1)–Mn(5)–O(6W)	107.1(5)
Mn(5)–O(1)	2.158(9)	O(3W)–Mn(3)–O(9)#1	109.0(3)	O(5W)–Mn(5)–O(6W)	87.3(7)
Mn(5)–O(5W)	2.161(19)	O(3W)–Mn(3)–O(9)	109.0(3)	O(38)#2–Mn(5)–O(6W)	155.9(5)
Mn(5)–O(38)#2	2.191(11)	O(9)#1–Mn(3)–O(9)	142.0(5)	O(39)#2–Mn(5)–O(6W)	81.1(5)
Mn(5)–O(39)#2	2.192(11)	O(3W)–Mn(3)–O(5)#1	108.8(2)	O(8W–Mn(6)–O(35)#1	140.6(5)
Mn(5)–O(6W)	2.226(13)	O(9)#1–Mn(3)–O(5)#1	86.1(4)	O(8W)–Mn(6)–O(35)	140.6(5)
Mn(6)–O(8W)	2.05(3)	O(9)–Mn(3)–O(5)#1	81.9(4)	O(35)#1–Mn(6) –O(35)	78.8(9)
Mn(6)–O(35)#1	2.166(2)	O(3W)–Mn(3)–O(5)	108.8(2)	O(8W)–Mn(6)–O(7W)#1	87.0(6)
Mn(6)–O(35)	2.166(2)	O(9)#1–Mn(3)–O(5)	81.9(4)	O(35)#1–Mn(6)–O(7W)#1	90.7(7)
Mn(6)–O(7W)	2.200(2)	O(9)–Mn(3)–O(5)	86.1(4)	O(35)–Mn(6)–O(7W)#1	94.0(7)
Mn(6)–O(7W)#1	2.200(2)	O(5)#1–Mn(3)–O(5)	142.5(5)	O(8W)–Mn(6)–O(7W)	87.0(6)
O(23)-Mn(1)-O(19)#1	78.8(4)	O(36)–Mn(4)–O(9)	139.2(4)	O(35)#1–Mn(6)–O(7W)	94.0(7)
O(23)–Mn(1)–O(26)	82.1(4)	O(36)–Mn(4)–O(5)#1	134.6(4)		
O(19)#1–Mn(1)–O(26)	131.7(4)	O(9)–Mn(4)–O(5)#1	78.7(4)		

Symmetry transformations used to generate equivalent atoms: #1 –x+1, y, –z+1/2; #2 x, –y–1, z+1/2; #3 x, –y–1, z–1/2.